Soft Matter

RSC Publishing

PAPER

View Article Online
View Journal | View Issue

Cite this: *Soft Matter*, 2013, **9**, 3651

Assembly of the anisotropic microcapsules in aqueous dispersions†

Milana Lisunova,[a] Andriy Dorokhin,[b] Neal Holland,[a] Valeriy V. Shevchenko[b] and Vladimir V. Tsukruk*[a]

Received 26th October 2012
Accepted 4th February 2013

DOI: 10.1039/c3sm00142c

www.rsc.org/softmatter

The assembly of cubic hollow microcapsules in an aqueous buffer solution had been studied in comparison with the traditional spherical microcapsules with both microcapsules assembled from identical components and having identical surface charges. We observed that the cubic microcapsules mainly form the highly compacted "boxed" clusters with a number of microcubes controlled by ionic strengths in a sharp contrast to the spherical microcapsules for which the random branched chain structures are generally favored. The assembled spherical microcapsules create a large number of openings with extensive internal surface areas while the cubic microcapsules build close, compacted aggregates with densely packed units. The dimensions of the "boxed" clusters from similarly charged cubic microcapsules are greatly stabilized by strong facet-to-facet interactions and can be tuned in a wide range by changing ionic strength. The chain spherical microcapsules are mobile and capable of reconfiguration due to the lower hydrophobic energy of attraction in contrast to compact, stable aggregates of cubic microcapsules. The dramatic differences in assembly of microcapsules *with similar nature but different shapes* point that the aggregation behavior in such dispersions might be dominated by shape geometry and alternation of facet-to-facet interactions.

Introduction

Ultrathin shell polymer microcapsules, which can be formed by the coating of selected cores followed by their dissolution, are proposed for applications in enzymatic catalysis and as a platform for the construction of artificial cells and organelles among many other applications.[1,2] Hollow microcapsules are of great interest because of their ability for *controlled high load storage/release* and potential to act as synthetic cell-like structures.[3–6] They possess unique characteristics that are extremely intriguing for further studies such as low specific density, high specific surface area, and potential for high loading capacity, high permeability, and enhanced catalytic and binding activities.[7–9] The advantage of these synthetic structures is that their properties can be tailored by designing responses to specific stimuli, which trigger the *release* of their content at a desired site and at a specific time.[10,11]

Layer-by-layer (LbL) assembly on various cores through a sequential adsorption of properly matched species – biological molecules, polymers, organic molecules, and nanoparticles – is one of the popular approaches enabling the formation of thin shell microcapsules and shells.[12–22] Spherical hollow microcapsules are frequently made using LbL assembly on organic/inorganic spherical templates such as polystyrene (PS) or silica (SiO_2) microparticles, which are dissolved after the deposition of the LbL coating.[13,23,24] On the other hand, a number of inorganic cores such as calcium carbonate ($CaCO_3$), manganese carbonate ($MnCO_3$), cadmium carbonate ($CdCO_3$), or tin sulfide (SnS) have been employed as anisotropic templates for the preparation of anisotropic hollow microcapsules.[25] Anisotropic microcapsules of a cubic shape with capsule walls made *via* the LbL approach have been recently demonstrated by Holt *et al.*[26] Cubic LbL microcapsules have been fabricated by the deposition of poly(methacrylic acid)/poly(*N*-vinylpyrrolidone) (PMAA/PVPON) or PMAA/poly(ethylene oxide) (PMAA/PEO) multilayers from pH 3.5 solutions onto the 10 μm cubic $CdCO_3$ particles.[27]

Remarkably, the original shape of the template particles was demonstrated to be perfectly preserved, including sharp edges, despite the ultrathin walls of a resultant capsule (less than 20 nm).[28] Moreover, these anisotropic hollow polymer microcapsules possess pH-sensitivity and can be quickly dissolved under basic conditions. The high stability of nanoscale shells also allows for reduction of the characteristic dimensions of the anisotropic microcapsules to a submicron scale (about 200 nm) with the preservation of a robust tetrahedral shape.[29] However, there are few examples where anisotropic, thin-shell LbL polymer microcapsules have been demonstrated, despite the fact

[a]*School of Materials Science and Engineering, Georgia Institute of Technology, Atlanta, Georgia 30332, USA. E-mail: Vladimir@mse.gatech.edu*

[b]*Institute of Macromolecular Chemistry, National Academy of Science of Ukraine, Kiev, 02160, Ukraine*

† Electronic supplementary information (ESI) available: Table 1S and confocal images of the guided assemblies. See DOI: 10.1039/c3sm00142c

that anisotropic shapes play a critical role in the organization of synthetic and natural structures into complex hierarchical assemblies.[30]

Assembly of various microparticles and microcapsules are a critically important process that plays a central role in the controlled drug delivery, cellular uptake, microfluidic delivery, and pH-regulating transport behavior in a fluidic environment.[31–34] Guided self-assembly of gels on patterned structures was used to create structures with different spatial arrangements.[35] Controllable assembly of hydrogel sheets at gas–liquid interfaces was performed to facilitate tissue engineering studies and fabricate micropatterned polyelectrolytes.[36,37] Despite some studies of anisotropic capsules in the fluidic environment, attempts to quantify aggregation behavior are rare because of technical challenges.

Most studies of aggregation behavior of microcapsules have considered spherical microcapsules and it is only more recently that nonspherical shapes (*e.g.* ellipsoids) have been investigated.[38,39] Understanding the organizing principles that lead to the *dense packing* of nonspherical particles that do not tile space is of great practical and fundamental interest.[39,40] On the theoretical side, recent simulation by Glotzer's group on the dense packing of tetrahedral particles shows that even subtle changes in shape can cause profound changes in the resulting ordered structure.[41] Moreover, not only the whole particle shape but also specifically shaped surface regions can control local arrangements.

Although there is emerging interest in uncovering how assembly processes are affected and modulated by shape changes of the building blocks. For instance, Kim *et al.* reported thermally responsive microcapsules with 25 nm diameter pores on the shell formed by hierarchical self-assembly of double tethered rod amphiphiles. Upon heating or cooling, the hydrophilic oligo-(ethylene-oxide) coils at one end of the rods shrink or expand, respectively, resulting in a reversible closed/open gating motion of the nanopores.[42] They also demonstrated a reversible transformation between two-dimensional sheets and tubular structures assembled by laterally grafted rod

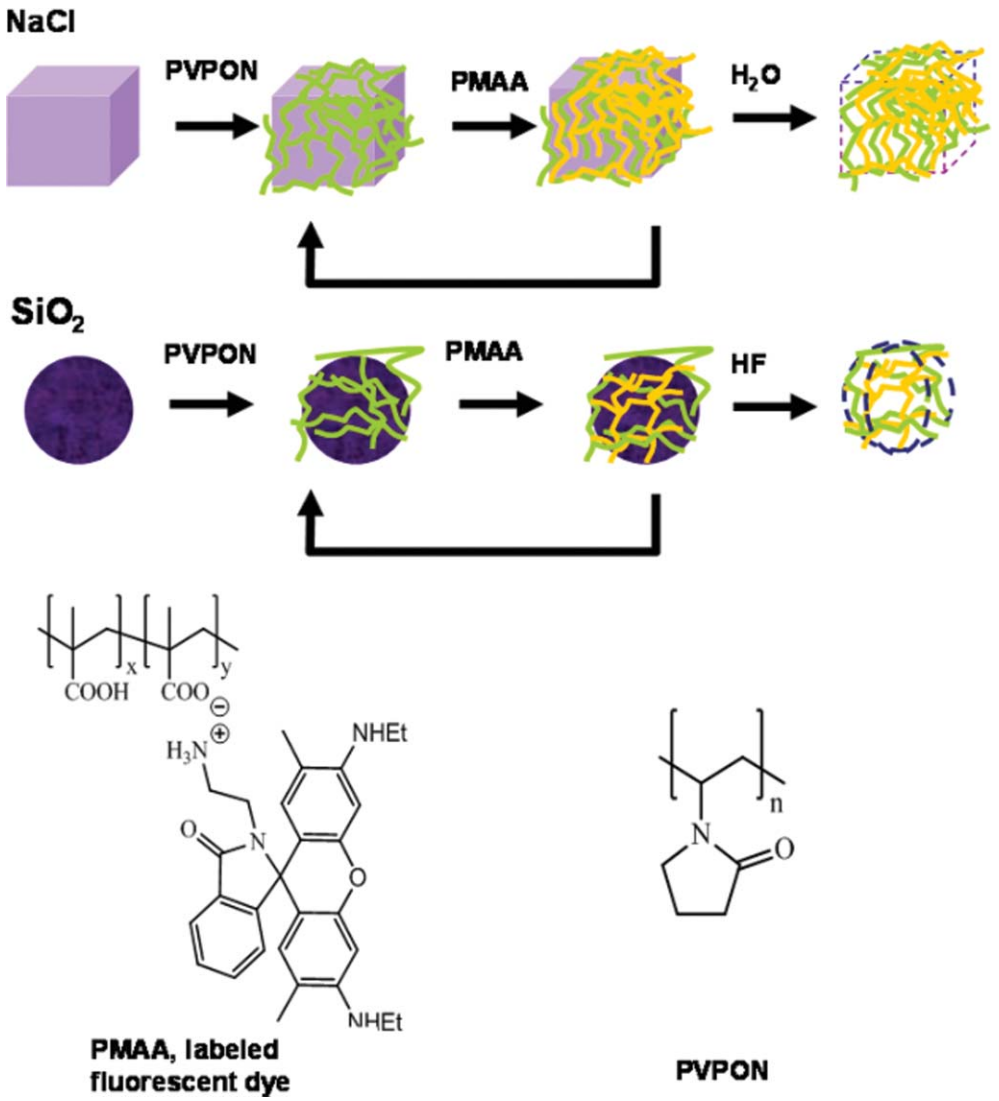

Fig. 1 Assembly of cubic and spherical microcapsules (top). Chemical structure of the PMAA labeled by a fluorescent dye, PVPON (bottom).

amphiphiles upon heating *via* a similar mechanism.[43] Recently, Zhang *et al.* have demonstrated that a simple cubic lattice of palladium nanocubes coated by dodecanethiol ligands in toluene transforms into a rhombohedral lattice upon solvent evaporation.[44] Change of the nanoparticle shape from cuboid to ellipsoid was attributed to the swelling of ligands as the solvent concentration decreased during evaporation.

Apart from magnetically driven interactions,[45] hydrogen-bonding assembly was applied to ligand-modified gold nanoparticles.[46] Yet another example involves assembly of tetrahedral CdTe nanocrystals into free-floating sheets *via* a combination of electrostatic and hydrogen-bonded interactions.[47] Granik constructed a Kagome lattice *via* the control of long-range electrostatic repulsion and short in-range hydrophobic bonded interactions.[48] Zhang *et al.* controlled the fusion of the assembled microcapsules *via* reduction of electrostatic repulsion and increase of polyelectrolyte shells interaction by adding high concentrations of salt.[49,50]

Here, we focus on revealing how the shape of microcapsules affects their aggregation behavior in solution by directly comparing the aggregation of spherical and cubic microcapsules with identical dimensions and composition by observing labeled microcapsules with confocal microscopy and particle counting. Specifically, LbL microcapsules with comparable dimensions and repulsive shells were synthesized from the hydrogen-bonded polymers on sodium chloride (NaCl) cubic cores and SiO_2 spherical cores, followed by a core release of water and acid, respectively (Fig. 1). We demonstrated that cubic and spherical microcapsules possess strikingly different aggregation behavior with stable, large, compact, and "boxed" aggregates formed by cubic microcapsules in contrast to mobile, chain-like aggregation of spherical microcapsules. Furthermore, the aggregation behavior can be further tuned by screening Coulombic interactions with the salty environment.

Results and discussion

The overall shape and fine morphology of collapsed hollow spherical and cubic LbL microcapsules has been observed in the dried state (see Fig. 2). AFM images show common collapsed morphology with random wrinkling as reported in earlier studies.[51] Confocal images of the spherical and cubic LbL microcapsules revealed the nearly monodisperse microcapsules with a dimension of 4 ± 1 μm (Fig. 2 and S1–S4†). The shell thickness in the dry state is within 10–12 nm and 18–20 nm for 4-bilayer spherical and cubic shells (see Fig. S5†), respectively. Such differences in wall thickness are introduced by core dissolution and release as has been discussed elsewhere.[52] In addition, the $(PVPON/PMAA)_4$ microcapsules did not change their dimensions at high ionic strength as was confirmed by confocal observations (ESI, S2†) and reported for LbL microcapsules.[51,53–55]

At low salt concentrations (<0.1 M) both cubic and spherical microcapsules are negatively charged due to the presence of a PMAA topmost layer with a surface potential from −16 to −22 mV (see Fig. 3). Thus, under these ionic conditions microcapsules are highly repulsive in solution and this repulsion prevents to a great extend their aggregations as indeed shown below. In contrast, at high salt concentrations (>0.1 M), the surface potential of microcapsules reaches 0 indicating their neutral state. Therefore, under these conditions the repulsive

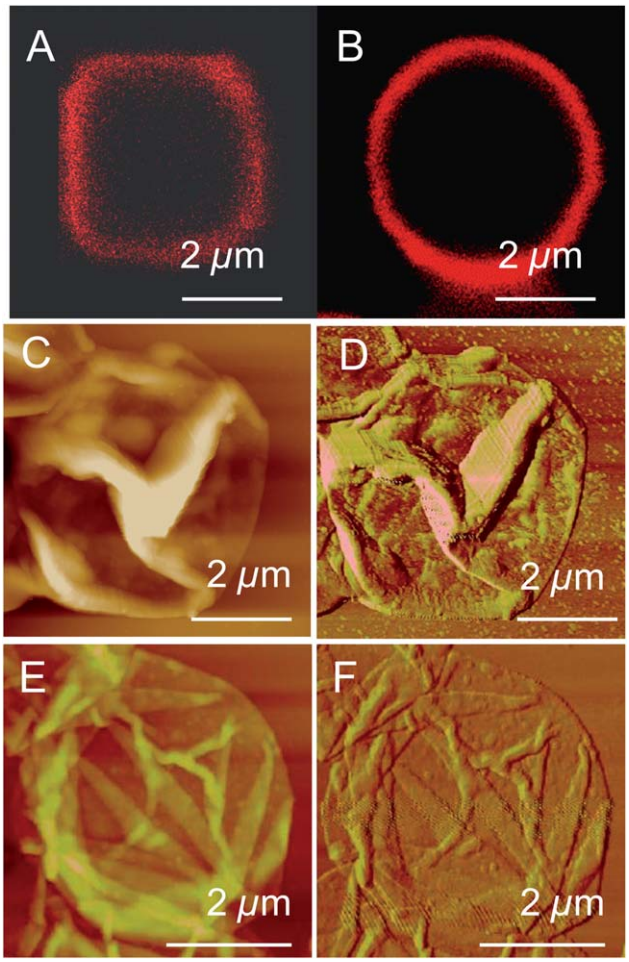

Fig. 2 Confocal images of cubic (A) and spherical (B) microcapsules. AFM topography (left) and phase (right) images of 4-bilayer cubic (C and D) and spherical (E and F) microcapsules. Z-scale is 600 nm (C) and 350 nm (E).

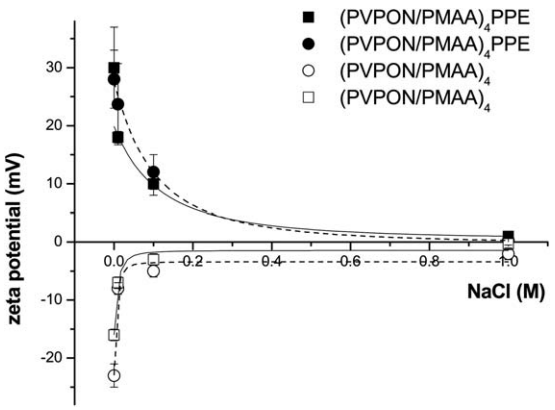

Fig. 3 Surface potential of cubic (□, ■) and spherical (○, ●) $(PVPON/PMAA)_4$ and $(PVPON/PMAA)_4PPE$ microcapsules *versus* the concentration of NaCl in buffer pH 4.5.

electrostatic forces are mostly suppressed and van der Waals forces play an important role in the aggregation behavior of microcapsules promoting aggregation. However, the aggregation behavior is dramatically different for cubic and spherical microcapsules as discussed below.

Indeed, confocal images of representative aggregates for cubic and spherical microcapsules show very different aggregation under high ionic strength conditions (Fig. 4 and 5). The spherical microcapsules show weak aggregation behavior with very few microcapsules observed in close contact at low ionic strength as well as formation of loose and the highly branched chain aggregates of neutral microcapsules at high ionic strength (Fig. 4, S6†). The aggregated spherical microcapsules are highly randomized with a large number of openings with extensive surface areas and limited point-like contacts of few neighboring microcapsules. The branched chain aggregates could be easily rearranged under mechanical stirring which is common for spherical microparticles with weak interparticle interactions.[56]

In high contrast, the cubic microcapsules form closed, very compact "boxed" aggregates which are stable and do not reorganize themselves with time (Fig. 5 and S7†). This remarkable difference in the aggregation behavior is getting more pronounced at higher ionic strength of dispersion with suppressed repulsion. Larger and stable aggregation is observed for neutral cubic microcapsules which form the highly compacted "boxed" cubic aggregates composed of an increasing number of multiple cubic microcapsules. These aggregates are stable and preserved over a large period of observation time (Fig. S7†).

Differences in the spherical and cubic microcapsules aggregation with statistical data from bulk dispersions can be quantified by analyzing the particle counter results (Fig. 6). This method allows for the reliable quantification of a large time and spatial scale in contrast to high resolution confocal images with a limited number of microcapsules observed in close proximity to substrates (not in a free volume). The volume distribution statistics of aggregated spherical and cubic microcapsules in

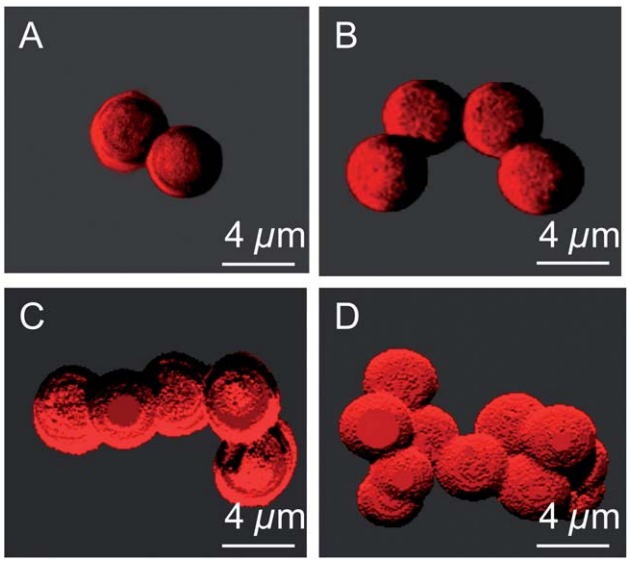

Fig. 4 Confocal images of three dimensional (3D) assemblies of spherical $(PVPON/PMAA)_4$ microcapsules in buffer pH 4.5, $C = 0.01$ M NaCl (A and B) and $C = 1$ M NaCl (C and D).

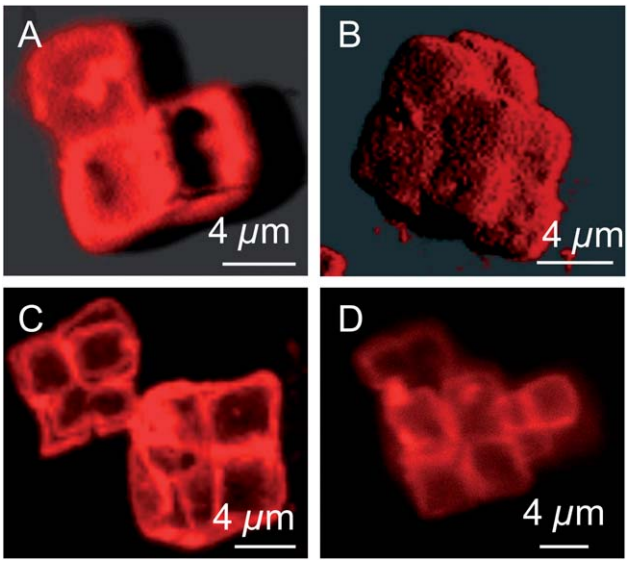

Fig. 5 Confocal images of cubic $(PVPON/PMAA)_4$ microcapsule assemblies in buffer at pH 4.5, $C = 0.01$ M NaCl (A and B) and $C = 1$ M NaCl (C and D).

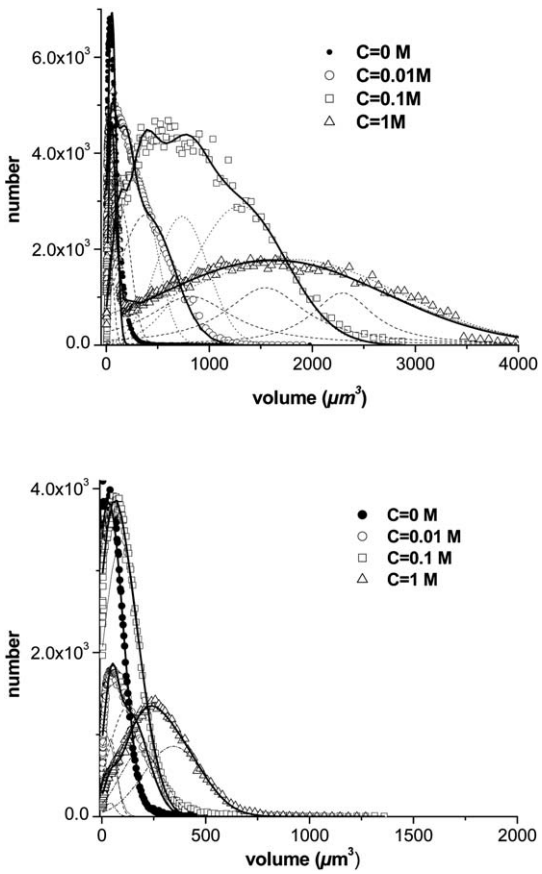

Fig. 6 Distribution aggregates of cubic (top) and spherical (bottom) microcapsules by volume. Dashed lines represent deconvoluted contributions. Pay attention to different *x*-scales for panels.

the aqueous buffer (pH = 3.5) show dramatic changes at different salt concentrations. At the initial state, 0 M, the volume distribution exhibits one peak for both types of microcapsules that corresponds to homogeneous distribution of the microcapsules in aqueous dispersion which corresponds to the predominant presence of individual microcapsules. The corresponding peak is sharp for cubic microcapsules although spherical microcapsules display a broader distribution indicating the minor presence of some dimers as well.

The appearance of the secondary volume distribution modes by adding NaCl evidences significant microcapsule aggregation with dimers, trimers and higher aggregated clusters contributing to broader maxima which are shifted to large volumes. It is worth noting that the increase of the aggregate volume is significantly larger (by a factor of 5) for cubic microcapsules. These trends confirm the conclusions made above from confocal observations of individual aggregates as discussed above.

For further quantification of an increase in the volume of aggregates with an increasing concentration of NaCl in aqueous dispersions of microcapsules we conducted the deconvolution of the peaks and their integration of the peak areas (see examples in Fig. 6). The analysis of component peaks allows for the evaluation of different contributions and direct estimation of the aggregation number (number of microcapsules in the average aggregate) by normalizing a total volume to the volume of a single microcapsule (Fig. 7). The volume of spherical and cubic microcapsules is about 34 μm^3 and 64 μm^3, respectively as evaluated from confocal images. These estimations show that in the highly charged state repulsive microcapsules are non-aggregated (one microcapsule per aggregate, Fig. 7). An increase in the ionic strength or dispersion (thus, decrease in repulsive surface charges) results in gradual aggregation of spherical microcapsules with dimers mostly formed for low salt concentration replaced with pentamers at a completely neutral state of spherical microcapsules at the highest salt concentration (Fig. 7). A similar trend in aggregation behavior is observed for cubic microcapsules but with much faster increase in the aggregation number from dimers to trimers at 0.01 M to around 20 (with broad distribution) in a completely neutral state which is 3 times higher than the aggregation number for spherical microcapsules (Fig. 7).

In order to estimate the effect of the facet-to-facet interactions on the aggregation behavior we estimated the interfacial energies involved in the inter-microcapsule interactions (Fig. 8).[57] As known, the interfacial free energy of per unit contact area ΔG^{ad} can be evaluated in accordance with the Dupre equation:[58,59]

$$\Delta G^{ad}_{132} = \gamma_{12} - \gamma_{13} - \gamma_{23} \quad (1)$$

where γ_{ij} is the interfacial free energy per unit area between phase i and j (Fig. 8). The energy components of the two surfaces in the aqueous dispersion can be calculated in accordance with usual approximation:[60]

$$\gamma_{ij} = \gamma_i + \gamma_j - 2\sqrt{\gamma_i^{LW}\gamma_j^{LW}} - 2\sqrt{\gamma_i^{+}\gamma_j^{-}} - 2\sqrt{\gamma_i^{-}\gamma_j^{+}} \quad (2)$$

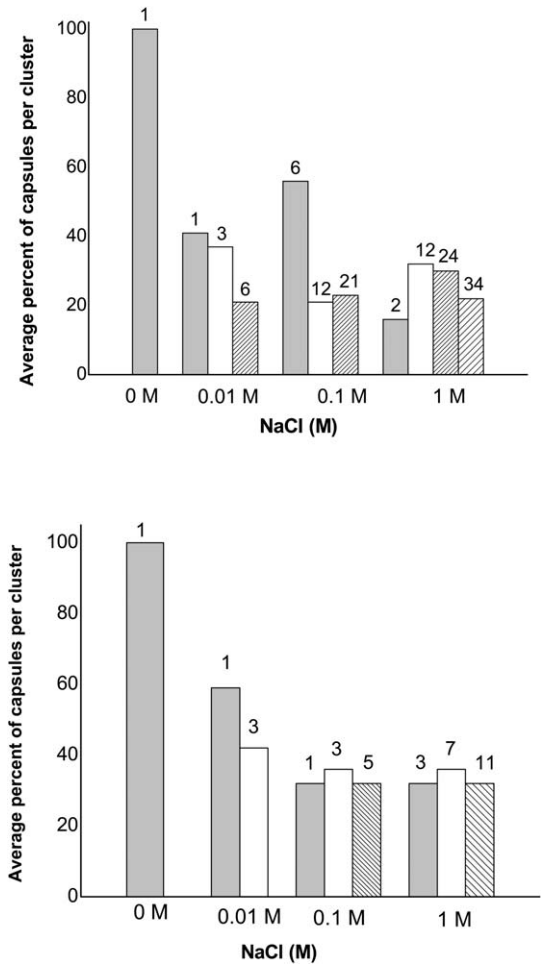

Fig. 7 Average percent of cubic (top) and spherical (bottom) microcapsules per aggregate *versus* the concentration of salt in an aqueous buffer at pH = 3.5.

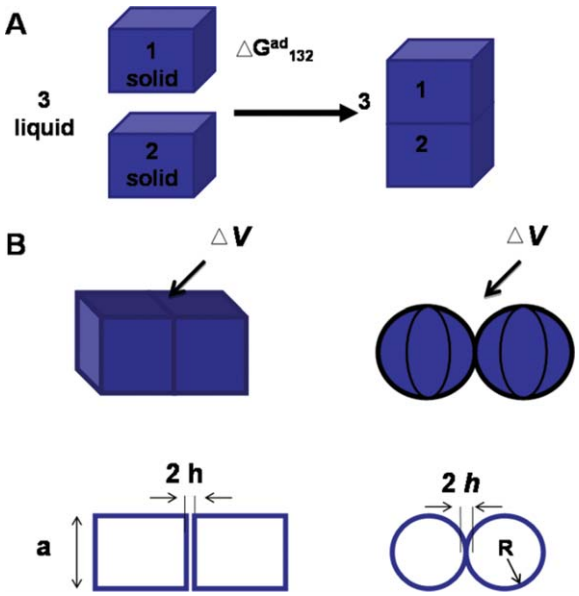

Fig. 8 Inter microcapsule (solid 1 and solid 2) interactions in aqueous buffer (liquid 3) (A). Interactions of the cubic–cubic (left) and spheres–spheres (right) microcapsules in aqueous buffer (B). ΔV is the overlapping excluded volume and h is the overlapping width of the interacting microcapsules.

where γ^{LW} is the van der Waals interaction component, γ^- is the acidic component, and γ^+ is the basic component.

The interfacial energies evaluated from eqn (1) and (2) with use of literature data (Table S1†) are summarized in Table 1.[61–63] The analysis of these data shows that the interfacial hydrophobic interactions for cubic microcapsules are four orders of magnitude higher in comparison to the spherical microcapsules mainly due to the differences in the contact surface area (S). Indeed, 16 μm^2 of the contact area for cubic microcapsules is dramatically higher than that for the spherical microparticles with a point-like contact area that varies from 10–100 nm^2 (as estimated from Fig. 4).[64] Note, that the contact surface area of spherical microcapsules may be affected by the mechanical deformation of the soft shells.[25,55,65] Indeed, our recent surface force spectroscopy studies demonstrated significant changes in compliance of LbL shells depending upon release conditions with elastic modulus varying widely in the MPa range.[25] The control of the contact surface area *via* variation of the mechanical stiffness (by changing properties of shells as well aqueous buffer) can be addressed in further investigations of the microcapsule assemblies.

According to Granick *et al.*, the results place the hydrophobic energy interaction around 10 k_BT (0.4×10^{-19} J) (where $k_B = 1.38 \times 10^{-23}$ J K^{-1} is the Boltzmann constant and T is the temperature) which allows the formation of the thermodynamically favorable product (or thermodynamically stable clusters).[56] Thereby, the assemblies built from spherical microcapsules, depending on the contact area (from 10 to 100 nm^2), could create either stable or mobile aggregates. Very stable aggregation with partial fusion (estimated interaction energy of 100–1000 k_BT) should be observed for a 100 nm^2 contact area and less stable, mobile branched aggregates are characteristics of microcapsules with small contact area (below 10 nm^2).[56] On the other hand, the high level of the hydrophobic interaction of the cubic microcapsules is characterized by a much higher energy around $\sim 10^7$ k_BT that should lead to the virtually irreversible stabilization of large aggregates with maximized hydrophobic contacts.

Although no shape-related changes in aggregation behavior have been reported, the increasing aggregation number with increasing dimensions of microparticles has been reported. The increasing size of the aggregates with increasing hydrophobic energy interactions (from 2 k_BT to 5 k_BT) due to the increasing size of particles (from 6 nm to 11 nm) was observed by Rijssel *et al.*[66] The increase in the thermodynamic energy of the interaction (ΔG) with increasing particle size was also reported by Hammond *et al.*[67] The energy of the particle adsorption increases from 20 k_BT to 50 k_BT with increasing particle size from 150 nm to 300 nm. The dimerization of the spherical particles through the control hydrophobic interaction and electrostatic repulsion of the particles during synthesis has been researched by the Xia group.[68] The dimer formation was observed when the electrostatic repulsion was reduced to -10 k_BT. Beyond the simplest case of the spherical microparticles examples where the strong hydrophobic forces resulted in directional interactions between anisotropic particles have been discussed. For instance, nanorods prefer to assemble side-by-side and not end-to-end when the ratio of the vdW energies for side-by-side/end-to-end is larger than unity.[69,70]

Nanorods form ordered phases at volume fractions in solution as low as $\varphi \sim 0.05$ since the excluded volume between two rods is much larger than the volume of the rods themselves. Simple analogy explains tendency of anisotropic cubic microcapsules to assemble into "boxed" aggregates while the spherical microcapsules at the same volume fraction ($\varphi \sim 0.1$) in aqueous buffer tend to form linear chain aggregates. According to Ming *et al.*[71] highly ordered super-structures from the microparticles are required to maintain the balance between the entropic depletion potential and electrostatic repulsion potential. Rossi *et al.* presented the possibility to form the close-packed mesostructures from the microcubes (1 μm) driven mainly by depleting polymer force coated microcubes.[72] Onsager *et al.*[73] have shown that the depleting potential of spherical particles becomes stronger when the contacting surface is planar or concave because of the larger increase in the solute free volume. According to Asakura the entropy depletion is significantly affected by the overlapping volume (ΔV) of the contacting particles (Fig. 8).[74] It is clear that facet particles possess a high length scale of the contact that consequently results in a more pronounced depletion attraction mechanism with, however, more research needed to clarify the role of this mechanism.

In order to estimate the effect of the electrostatic interactions, we evaluated the electrostatic interactions, ΔV^e, between the microcapsules with linear superposition approximation:[67,75]

$$\Delta V^e \approx \varepsilon \Psi_{par} \Psi_{temp} \frac{R_1 R_2}{L} e^{-k(L-R_1-R_2)} \quad (3)$$

where ε is the dielectric constant of the media, $1/k$ is the characteristic Debye–Hückel length, R_1 and R_2 are the radii of the interacting particles, L is the distance between the interacting microparticles, and Ψ_1 and Ψ_2 are the surface potentials of the particles. To apply this estimation to our systems, we assume that the distance between two interacting microcapsules is much larger than microcapsule dimensions ($R_o = 2$ μm). The effective radius of the cubic microcapsules was estimated as $\sqrt{3}/2a$ ($R_\square = 3.48$ μm). Zeta potential values were utilized as estimated earlier (Fig. 5). The analysis of these data shows that the electrostatic energy for spherical microcapsules is comparable to hydrophobic forces in close contact evaluated above (Table 1). In contrast, the hydrophobic energy for cubic microcapsules in close contact is four-order of magnitude higher than

Table 1 The hydrophobic ΔW^a and electrostatic ΔV^e interfacial energies, contact surface area S between the microcapsules calculated in accordance with eqn (1) and (3), respectively

Surfaces	S (μm^2)	ΔG^{ad} (mJ m^{-2})	ΔW^a (J)	ΔV^e (J)
Cubic PMAA/PMAA	16	−43	-68.8×10^{-14}	$+5.22 \times 10^{-18}$
Spherical PMAA/PMAA	0.01–0.1	−43	-4.3×10^{-19} to -4.3×10^{-17}	$+3 \times 10^{-18}$

the repulsive Coulombic interactions thus facilitating reduction of free energy of aggregated dispersions.

Finally, in order to further test the binding interactions between the microcapsules with opposite surface potentials the positively charged poly(*p*-phenylene ethynylene) (PPE) polymer shells were assembled on the $(PVPON/PMAA)_4$ microcapsules that resulted in surface potential changing sign from −20 mV to +30 mV (Fig. 3). These oppositely charged microcapsules were mixed in dispersion and the aggregation behavior was monitored with confocal microscopy and with a particle counter (Fig. 9 and 10).

Surprisingly, we did not observe any significant changes in the aggregation behavior for such mixed dispersion with large scale aggregation of oppositely charged microcapsules. Confocal images show weakly aggregated red (positively charged) and green (negatively charged) microcapsules without large scale aggregation (Fig. 9, S3 and S4†). Both spherical and cubic microcapsules formed very small aggregates composed of mostly dimers (spherical microcapsules) and quadmers (cubic microcapsules) under no-salt conditions (Fig. 11). We suggest that such initial aggregation may lead to charge compensation of aggregated microcapsules which prevents further Coulombic-interaction driven aggregation in larger aggregates. Aggregation increases with screening Coulombic interactions as was observed above with maximum aggregation number for oppositely charged spherical microcapsules being pentamers (Fig. 11). Again, the aggregation number increases even more for cubic microcapsules with a maximum of about 18 cubes, reaching a salt concentration of 1 M which is close to that observed for similarly charged cubic microcapsules (Fig. 11).

In conclusion, we have observed very different aggregation behavior of spherical and cubic LbL microcapsules with variable surface potentials in aqueous buffer. The difference in aggregation behavior of cubic (stable "boxed" dense packing with larger aggregation numbers) and spherical (mobile branched, open chain-like aggregation) microcapsules was related to the fact that the hydrophobic attraction energy of interaction between the cubic microcapsules are much higher than that for the spherical microcapsules due to the significantly higher facet-to-facet contact surface area of cubic microparticles. In order to directly compare the aggregation behavior, in this study, we kept the composition and

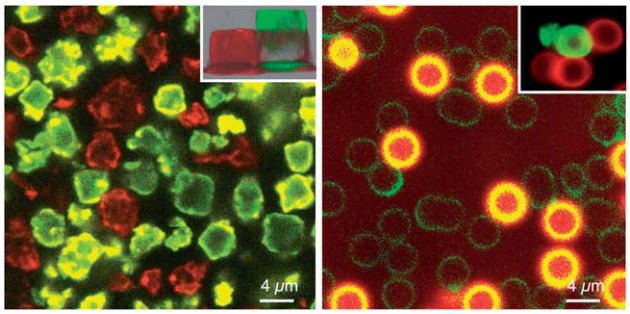

Fig. 9 Confocal images of assembled cubic (left) and spherical (right) $(PVPON/PMAA)_4$ and $(PVPON/PMAA)_4PPE$ microcapsules in buffer at pH 3.5, $C = 0.01$ M NaCl.

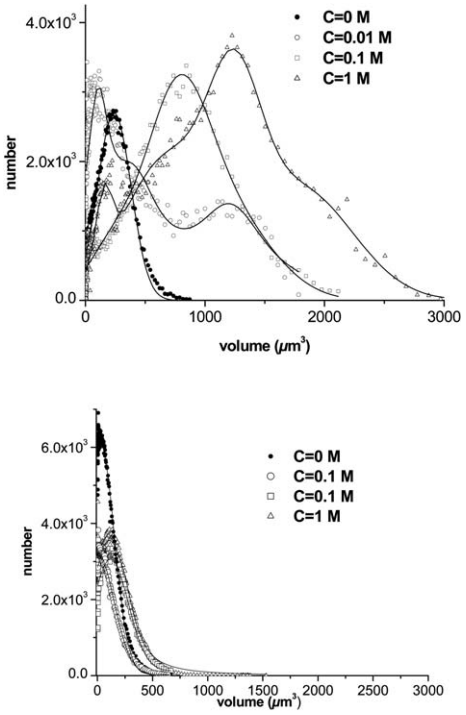

Fig. 10 Distribution aggregates of oppositely charged cubic (top) and spherical (bottom) microcapsules by volume.

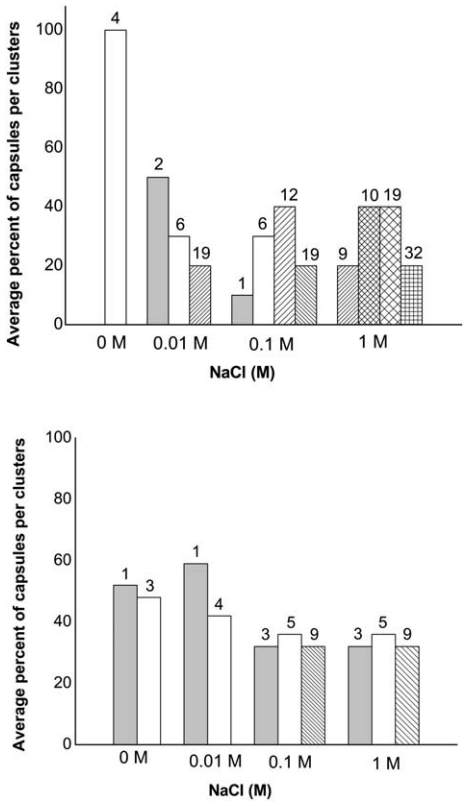

Fig. 11 Aggregation numbers of cubic (top) and spherical (bottom) microcapsules per clusters *versus* the concentration of salt in aqueous buffer pH = 3.5.

assembling routines for both spherical and cubic microcapsules identical, their dimensions very close, and surface charge states very similar. However, other secondary parameters such as solvents used for release, nature of sacrificial core microparticles, local microroughness, different thickness and porosity of shells, all might affect the fine details of aggregation behavior. Unfortunately, it is next to impossible to have all these parameters absolutely identical and their contribution into aggregation behavior still remains unclear at this stage and should be further explored.

The aggregated mobile spherical microcapsules create a large number of openings with extensive surface areas while the cubic microcapsules build close-packed aggregates. Similar aggregation behavior of cubic microcapsules in dispersions with high ionic strength disregarding initial surface potentials shows that aggregation can be mainly governed by shape geometry and strong-weak facet-to-facet interactions which makes the whole situation very different from traditional dispersion of spherical microparticles and makes these aggregations interesting for colloidal and surface phenomena important for microfluidic flows, adsorption on heterogeneous surfaces, clogging behavior, and controlling delivery and transport phenomena in complex media.

Experimental

Materials

Poly(methacrylic acid) (PMAA) with molecular weight (M_w) = 100 kDa, PVPON (1300 kDa), and sodium chloride were purchased from Sigma-Aldrich. Poly(*p*-phenylene ethynylene) (PPE) with a molecular weight of 11 kDa utilized in this study was prepared as reported.[76,77] Dimethylformamide (DMF) and poly(methacrylic acid) (PMAA), M_w = 100 kDa, were purchased from Sigma-Aldrich. Silica particles with diameter 4.0 ± 0.2 μm as 10% dispersions in water were obtained from Polysciences, Inc. Ultrapure water (Nanopure system) with a resistivity of 18.2 MΩ cm was used in all experiments.

Preparation of salt NaCl core

200 mL NaCl solution (5 M) was added into 25 mL anhydrous ethanol with vigorous stirring, immediately giving a cloudy solution indicating the formation of NaCl crystals.[78]

Synthesis of the labeled PMAA

0.5400 g (6273 meq.) of PMAA was dissolved in 10 mL of DMF at 100 °C, and a solution of 0.1147 g (0.251 meq.) of 2-(2-aminoethyl)-3′,6′-bis(ethylamino)-2′,7′-dimethylspiro[isoindoline-1,9′-xanthen]-3-one in 3 mL of DMF was added while vigorous stirring (NH_2/COOH = 1/25). The main criteria to choose the mentioned ratio between amino- and carboxylic groups were the highest contrast of confocal images and suitable solubility of the final compound.

Preparation of LbL microcapsules

The LbL deposition of $(PVPON/PMAA)_4$ multilayers has been performed according to the established procedure described elsewhere (Fig. 1).[51] For deposition of $(PVPON/PMAA)_4$ multilayers on spherical cores, 0.5 mg mL^{-1} of each polymer solution was prepared by dissolving the polymers in an aqueous buffer with pH adjusted to 3.5. For deposition of $(PVPON/PMAA)_4$ multilayers on cubic NaCl cores, 0.5 mg mL^{-1} of each polymer solution was prepared by dissolving the polymers in an ethanol.[79] Typical deposition time on a single cycle was 15 min followed by three rinsing steps with solvent to remove excess free polymer. The polymer layers were coated one after the other. For microparticle suspensions, after each deposition step they were settled down by centrifugation at 2000 rpm for 2 min to remove the excess polymer. Deposition, rinsing and re-suspending steps were performed on a VWR analog vortex mixer at 2000 rpm. For PPE-containing LbL assembly, a layer of PPE was adsorbed after adsorption of the $(PVPON/PMAA)_4$ shell. After each deposition step particles were settled down by centrifugation at 2000 rpm for 2 min to remove the excess of polymer.

To etch out silica cores, the microparticles with the deposited multilayers were exposed to 8% hydrofluoric acid solution (HF) (*hazardous!*) overnight followed by dialysis in Nanopure water for 36 h with repeated change of water. The NaCl cores were dissolved by shaking the coated particle dispersion in an aqueous buffer at pH = 3.5 yielding LbL shaped hollow microcapsules. The dispersions of the microcapsules were then dialyzed against water for 3 days. The confocal and counter measurements were conducted for 2 hours after vigorously stirring the microcapsules in an aqueous buffer at pH = 3.5 at different concentrations of salt, that varied from 0 to 1 M NaCl. According to Pechenkin *et al.* NaCl does not induce any changes in microcapsules up to saturation concentration (6.1 M).[53] Note that the dispersions stay stable for several days.

Measurements

Surface potentials of the microparticles in aqueous solutions were measured on a Zetasizer nano-ZS (Malvern). Each value of zeta-potential was obtained under ambient conditions by averaging three independent measurements of 35 runs each. For atomic force microscopy (AFM) imaging, topographical and phase images of the surface morphology of dried microcapsules were observed under ambient conditions in the taping and phase modes in air, respectively, using an Icon AFM microscope (Bruker) according to established procedures.[80–82] Confocal images of microcapsules were obtained with a LSM 510 NLO META UV Vis inverted confocal laser scanning microscope (CLSM) equipped with 63 × 1.4 oil immersion objective lens (Zeiss). The excitation/emission wavelengths for the PPE (green) and labeled PMAA (red) were 488/515 and 543/560 nm, respectively. A drop of a dispersion of hollow microcapsules was added to several Lab-Tek chambers (Electron Microscopy Sciences), which were then filled with aqueous solutions.

The aggregate distribution of cubic and spherical microcapsules by volume was determined using a Coulter Multisizer III (Beckman Coulter Multisizer III, Coulter Corp.). The range of volumes detected is determined by the size of the aperture used for measurement, with the measured size ranging approximately 2–60% of the aperture diameter. An aperture tube with a

diameter of 30 μm was typically used.[83] The aperture of the instrument was calibrated using microsphere standards following the manufacturer's procedure.[84,85] The sample had been stirred carefully before the volume of microcapsules was measured. 0.01 g of microcapsules was dispersed into 10 mL aqueous buffer pH = 3.5 at different salt (NaCl) concentrations (C = 0–1 M). The microcapsule volume distribution curves were integrated using curve fitting of the peaks. The most consistent results were obtained when peaks were assumed to be Gaussian. The peak centers and bandwidths were not fixed, but the results of the curve fitting were carefully monitored for consistency in these parameters. The numbers of the microcapsules in assembled clusters were recalculated in terms of aggregation numbers by comparing the total volume measured to the volume of a single microcapsule.

Acknowledgements

This work was supported by the U.S. Department of Energy, Office of Basic Energy Sciences, Division of Materials Sciences and Engineering under Award # DE-FG02-09ER46604. We thank Prof. M. El-Sayed and Prof. U. H.F. Bunz for providing PPE.

References

1 G. B. Sukhorukov, A. L. Rogach, M. Garstka, S. Springer, W. J. Parak, A. Munoz-Javier, O. Kreft, A. G. Skirtach, A. S. Susha, Y. Ramaye, R. Palankar and M. Winterhalter, *Small*, 2007, **3**, 944.
2 B. Stadler, A. D. Price, R. Chandrawati, L. Hosta-Rigau, A. N. Zelikin and F. Caruso, *Nanoscale*, 2009, **1**, 68.
3 F. Caruso, D. Trau, H. Mohwald and R. Renneberg, *Langmuir*, 2000, **16**, 1485.
4 E. Donath, G. B. Sukhorukov, F. Caruso, S. A. Davis and H. Mohwald, *Angew. Chem., Int. Ed.*, 1998, **37**, 2202.
5 A. Hua, J. A. Steven and Y. M. Lvov, *Cell Biochem. Biophys.*, 2003, **39**, 23.
6 R. F. Fakhrullin, A. I. Zamaleeva, R. T. Minullina, S. A. Konnova and V. N. Paunov, *Chem. Soc. Rev.*, 2012, **41**, 4189.
7 X. W. Lou, L. A. Archer and Z. C. Yang, *Adv. Mater.*, 2008, **20**, 3987.
8 C. J. Martinez, B. Hockey, C. B. Montgomery and S. Semancik, *Langmuir*, 2005, **21**, 7937.
9 X. W. Lou, Y. Wang, C. L. Yuan, J. Y. Lee and L. A. Archer, *Adv. Mater.*, 2006, **18**, 2325.
10 M. Delcea, A. Yashchenok, K. Videnova, O. Kreft, H. Mohwald and A. G. Skirtach, *Macromol. Biosci.*, 2010, **10**, 465.
11 D. G. Shchukin, T. Shutava, E. Shchukinsa, G. B. Sukhorukov and Y. M. Lvov, *Chem. Mater.*, 2004, **16**, 3446.
12 V. Khutoryanskiy, *Int. J. Pharm.*, 2007, **334**, 15.
13 E. Kharlampieva and S. A. Sukhishvili, *J. Macromol. Sci.*, 2006, **46**, 377.
14 P. Lavalle, J. C. Voegel, D. Vautier, B. Senger, P. Schaaf and V. Ball, *Adv. Mater.*, 2011, **23**, 1191.
15 J. E. Quinn and F. Caruso, *Aust. J. Chem.*, 2005, **58**, 442.
16 V. Kozlovskaya, S. Harbaugh, I. Drachuk, O. Shchepelina, N. Kelley-Loughnane, M. Stone and V. V. Tsukruk, *Soft Matter*, 2011, **7**, 2364.
17 M. Lisunova, M. Mahmoud, N. Holland, Z. Combs, M. A. El-Sayed and V. V. Tsukruk, *J. Mater. Chem.*, 2012, **22**, 16745.
18 O. Shchepelina, I. Drachuk, M. K. Gupta, J. Lin and V. V. Tsukruk, *Adv. Mater.*, 2011, **23**, 4655.
19 J. T. Wilson, W. Cui, V. Kozlovskaya, E. Kharlampieva, D. Pan, Z. Qu, V. R. Krishnamurthy, J. Mets, V. Kumar, J. Wen, Y. Song, V. V. Tsukruk and E. L. Chaikof, *J. Am. Chem. Soc.*, 2011, **133**, 7054.
20 J. L. Carter, I. Drachuk, S. Harbaugh, N. Kelley-Loughnane, M. Stone and V. V. Tsukruk, *Macromol. Biosci.*, 2011, **11**, 1244.
21 R. Kodiyath, J. Wang, Z. A. Combs, S. Chang, M. K. Gupta, K. D. Anderson, R. J. Brown and V. V. Tsukruk, *Small*, 2011, **7**, 3452.
22 C. Ye, O. Shchepelina, R. Calabrese, I. Drachuk, D. L. Kaplan and V. V. Tsukruk, *Biomacromolecules*, 2011, **12**, 4319.
23 A. S. Angelatos, K. Katagiri and F. Caruso, *Soft Matter*, 2006, **2**, 18.
24 C. Y. Jiang and V. V. Tsukruk, *Adv. Mater.*, 2006, **18**, 829.
25 O. Shchepelina, M. O. Lisunova, I. Drachuk and V. V. Tsukruk, *Chem. Mater.*, 2012, **24**, 1245.
26 B. Holt, R. Lam, F. C. Meldrum, S. D. Stoyanov and V. N. Paunov, *Soft Matter*, 2007, **3**, 188.
27 V. Kozlovskaya, S. Yakovlev, M. Libera and S. A. Sukhishvili, *Macromolecules*, 2005, **38**, 4828.
28 O. Shchepelina, V. Kozlovskaya, S. Singamaneni, E. Kharlampieva and V. V. Tsukruk, *J. Mater. Chem.*, 2010, **20**, 6587.
29 O. Shchepelina, V. Kozlovskaya, E. Kharlampieva, W. Mao, A. Alexeev and V. V. Tsukruk, *Macromol. Rapid Commun.*, 2010, **23**, 2041.
30 M. Lisunova, N. Holland, O. Shchepelina and V. V. Tsukruk, *Langmuir*, 2012, **28**, 13345.
31 S. C. Glotzer and M. L. Solomon, *Nat. Mater.*, 2007, **6**, 557.
32 E. Ruiz-Hitzky, M. Darder, P. Aranda and K. Ariga, *Adv. Mater.*, 2010, **22**, 323.
33 V. V. Tsukruk, *Prog. Polym. Sci.*, 1997, **22**, 247.
34 M. C. Stuart, W. Huck, J. Genzer, M. Muller, C. Ober, M. Stamm, G. Sukhorukov, I. Szleifer, V. V. Tsukruk, M. Urban, F. Winnik, S. Zauscher, I. Luzinov and S. Minko, *Nat. Mater.*, 2010, **9**, 101.
35 S. Hiltl, M. P. Schurings, A. Balaceanu, V. Mayorga, C. Liedel, A. Pich and A. Boker, *Soft Matter*, 2011, **7**, 8231.
36 B. Zamanian, M. Masaeli, J. W. Nichol, M. Khabiry, M. J. Hancock, H. Bae and A. Khademhosseini, *Small*, 2010, **6**, 937.
37 D. G. Shchukin, D. S. Kommireddy, Y. Zhao, T. Cui, G. B. Sukhorukov and Y. M. Lvov, *Adv. Mater.*, 2004, **16**, 389.
38 Y. Jiao, F. H. Stillinger and S. Torquato, *Phys. Rev. E: Stat., Nonlinear, Soft Matter Phys.*, 2009, **79**, 041309.
39 A. Donev, F. H. Stillinger, P. M. Chaikin and S. Torquato, *Phys. Rev. Lett.*, 2004, **92**, 255506.
40 J. H. Conway and S. Torquato, *Proc. Natl. Acad. Sci. U. S. A.*, 2006, **103**, 10612.

41 P. F. Damasceno, M. Engel and S. C. Glotzer, *ACS Nano*, 2012, **6**, 609.
42 J. K. Kim, E. Lee, Y. B. Lim and M. Lee, *Angew. Chem., Int. Ed.*, 2008, **47**, 4662.
43 E. Lee, J. K. Kim and M. Lee, *Angew. Chem., Int. Ed.*, 2009, **48**, 3657.
44 Y. Zhang, F. Lu, D. Lelie and O. Gang, *Phys. Rev. Lett.*, 2011, **107**, 135701.
45 A. Ahniyaz, Y. Sakamoto and L. Bergström, *Proc. Natl. Acad. Sci. U. S. A.*, 2007, **104**, 17570.
46 L. Han, M. M. Maye, F. L. Leibowitz, N. K. Ly and C. J. Zhong, *J. Mater. Chem.*, 2001, **11**, 1259.
47 Z. Tang, Z. Zhang, Y. Wang, S. C. Glotzer and N. A. Kotov, *Science*, 2006, **314**, 274.
48 Q. Chen, S. C. Bae and S. Granick, *Nature*, 2011, **469**, 381.
49 R. J. Zhang, K. Kohler, O. Kreft, A. Skirtach, H. Mohwald and G. Sukhorukov, *Soft Matter*, 2010, **6**, 4742.
50 M. A. Pechenkin, H. Mohwald and D. V. Volodkin, *Soft Matter*, 2012, **8**, 8659.
51 V. Kozlovskaya, E. Kharlampieva, I. Drachuk, D. V. Cheng and V. Tsukruk, *Soft Matter*, 2010, **6**, 3596.
52 O. Shchepelina, M. O. Lisunova, I. Drachuk and V. V. Tsukruk, *Chem. Mater.*, 2012, **24**, 1245.
53 M. A. Pechenkin, H. Mohwald and D. V. Volodkin, *Soft Matter*, 2012, **8**, 8659.
54 Q. Chen, J. K. Whitmer, S. Jiang, S. C. Bae, E. Luijten and S. Granick, *Science*, 2011, **131**, 199.
55 M. O. Lisunova, I. Drachuk, O. A. Shchepelina, K. D. Anderson and V. V. Tsukruk, *Langmuir*, 2011, **27**, 11157.
56 L. Hong, A. Cacciuto, E. Luijten and S. Granick, *Langmuir*, 2008, **24**, 621.
57 H. Onoe, K. Matsumoto and I. Shimoyama, *J. Microelectromech. Syst.*, 2004, **13**, 603.
58 C. J. van Oss, R. J. Good and M. K. Chaudhury, *J. Colloid Interface Sci.*, 1986, **111**, 378.
59 C. J. van Oss, R. J. Good and M. K. Chaudhury, *Langmuir*, 1988, **4**, 884.
60 L. A. Girifalco and R. J. Good, *J. Phys. Chem.*, 1957, **61**, 904.
61 R. J. Good, in *Contact Angle, Wettability and Adhesion*, ed. K. L. Mittal and V. S. P. Utrecht, The Netherlands, 1993, pp. 3–36.
62 S. Wu, *Org. Coat. Plast. Chem.*, 1971, **31**, 27.
63 L. H. Lee, in *Preprints, Div. Organic Coatings and Plastics Chemistry*, 154th National Meeting of ACS, Chicago, 1967.
64 V. V. Tsukruk and S. Singamaneni, in *Scanning Probe Microscopy of Soft Matter: Fundamentals and Practices*, Wiley-VCH, Weinheim, 2012.
65 I. Drachuk, O. Shchepelina, M. Lisunova, S. Harbaugh, N. Kelley-Loughnane, M. Stone and V. V. Tsukruk, *ACS Nano*, 2012, **6**, 4266.
66 J. van Rijssel, B. H. Erné, J. D. Meeldijk, M. Casavola, D. Vanmaekelbergh, A. Meijerink and A. P. Philipse, *Phys. Chem. Chem. Phys.*, 2011, **13**, 12770.
67 Y. H. Kim, J. Park and P. T. Hammond, *Adv. Mater.*, 2007, **19**, 4426.
68 M. Ibisate, Z. Zou and Y. Xia, *Adv. Funct. Mater.*, 2006, **16**, 1627.
69 K. J. M. Bishop, C. E. Wilmer, S. Soh and B. A. Grzybowski, *Small*, 2009, **5**, 1600.
70 T. K. Sau and C. J. Murphy, *Langmuir*, 2005, **21**, 2923.
71 T. Ming, X. Kou, H. Chen, T. Wang, H. L. Tam, K. W. Cheah, J. Y. Chen and J. Wang, *Angew. Chem., Int. Ed.*, 2008, **47**, 9685.
72 L. Rossi, S. Sacanna, W. T. M. Irvine, P. M. Chaikin, D. J. Pine and A. Philipse, *Soft Matter*, 2011, **7**, 4139.
73 L. Onsager, *Ann. N. Y. Acad. Sci.*, 1949, **51**, 627.
74 S. Asakura and F. Oosawa, *J. Polym. Sci.*, 1958, **33**, 183.
75 J. Aizenberg, P. V. Braun and P. Wiltzius, *Phys. Rev. Lett.*, 2000, **84**, 2997.
76 M. A. Mahmoud, A. J. Poncheri, R. L. Phillips and M. A. El-Sayed, *J. Am. Chem. Soc.*, 2010, **132**, 2633.
77 I. B. Kim, H. S. Shin, A. J. Garcia and U. H. F. Bunz, *Bioconjugate Chem.*, 2007, **18**, 815.
78 A. Janecovic and E. Matijevic, *J. Colloid Interface Sci.*, 1985, **103**, 436.
79 S. Beyer, W. C. Mak and D. Trau, *Langmuir*, 2007, **23**, 8827.
80 V. V. Tsukruk and D. H. Reneker, *Polymer*, 1995, **36**, 1791.
81 M. E. McConney, S. Singamaneni and V. V. Tsukruk, *Polym. Rev.*, 2010, **50**, 235.
82 V. V. Tsukruk, Z. Huang, S. A. Chizhik and V. V. Gorbunov, *J. Mater. Sci.*, 1998, **33**, 4905.
83 R. A. Reynolds, D. Stramski, V. M. Wright and S. B. Wozniak, *J. Geophys. Res.*, 2010, **115**, C08024.
84 L. Y. Chu, S. H. Park, T. Yamaguchi and S. Nakao, *Langmuir*, 2002, **18**, 1856.
85 S. M. Mirabedini, I. Dutil and R. R. Farnood, *Colloids Surf., A*, 2012, **394**, 74.

